Model-Based Analysis of UAV Accurate Landing in Stochastic Turbulent Environments

Zhanghao Lu*, Yuan Tang, Lutong Li, Renbo Su, Zhengyi Jiang, Simon Watson†, and Andrew Weightman‡
Manchester Centre for Robotics and AI, University of Manchester, Oxford road, Manchester

ABSTRACT

Deploying Inspection, Maintenance, and Repair (IMR) robots using unmanned aerial vehicles (UAVs) has emerged as a promising method for wind turbine blade inspection due to lower costs and higher accuracy. However, deploying these robots remains a challenge due to the high-speed, turbulent wind environments around wind farms, making it difficult for UAVs to land on turbine blades accurately. Using a novel discrete stochastic turbulent wind field model, this study evaluates a landing strategy for UAVs to land at higher speeds compared to typical UAV landing speed ($\leq$ 0.5 m/s) in turbulent wind fields to minimise lateral landing errors. Based on 4800 simulations performed at various wind speeds (3.0 - 12.0 m/s) and UAV landing speeds (0.5 - 3.0 m/s), it was observed that this landing strategy provides lower mean landing errors (up to 37.7%) compared to existing UAV landing systems when the wind speed is below 9 m/s, improving landing success rates by up to 30%.

1 INTRODUCTION

In recent decades, offshore wind farms have gained momentum due to fewer land-use constraints and access to stronger, more consistent winds compared to onshore wind farms [1]. However, the harsh marine environment has increased the demand for blade inspection, maintenance and repair (IMR), with blade damage being the most frequent and costly [2].

Traditional manual methods for offshore inspection are risky and expensive due to the unique geographical location [3]. Although UAVs offer promising solutions for remote blade inspection [4], they still face key limitations such as flight instability in turbulence, limited inspection accuracy, and battery capacity constraints. Moreover, maintenance and repair still require manual intervention, limiting full automation and cost reduction.

To address these challenges, a multi-robot platform was proposed in [3], where UAVs deploy and retrieve IMR robots for close-contact blade tasks. Among the mission phases, the landing poses the highest risk due to direct contact between the UAV and the blade under potentially high-speed turbulent environments.

*Email address: zhanghao.lu@student.manchester.ac.uk
†Email address: simon.watson@manchester.ac.uk
‡Email address: andrew.weightman@manchester.ac.uk

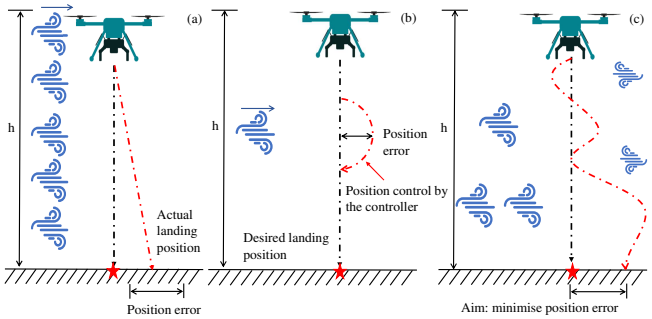

Figure 1: The illustration of the impact of (a) constant wind, (b) wind gusts and (c) wind turbulence on the positional error of the UAV.

The risks primarily arise from two factors: (1) lateral displacement caused by gusts and turbulence, which can reduce landing accuracy or lead to a landing near the blade edge, potentially causing the UAV to fall or collide with surrounding structures; and (2) vertical shear that might increase descent speed, resulting in elevated impact energy and contact forces, posing a risk of damaging both the UAV and the blade. While most existing studies adopt low descent speeds (typically $\leq$ 0.5 m/s), which allow sufficient time to compensate for gust-induced deviations [5], such approaches may be inadequate in highly turbulent conditions where wind speed and direction vary rapidly. Therefore, this study proposes a hypothesis that increasing descent speed can reduce the UAV's exposure time to wind disturbances and thereby improve landing accuracy, if the kinetic energy can be adequately dissipated during the landing process. To validate this hypothesis, we developed a simulation framework with a UAV platform and a height-varying stochastic turbulence field to evaluate landing performance across multiple wind and descent speed scenarios.

1.1 Background and Related Work

As illustrated in Figure 1, wind disturbances affecting UAV landing can be broadly classified into constant wind, gusts, and turbulence [6]. Constant wind refers to steady airflow that causes persistent deviations from the intended path, while gusts are short-term variations in speed and direction that lead to temporary trajectory shifts. Turbulence, the most

http://www.imavs.org/

http://www.imavs.org/

complex type, involves chaotic multidirectional fluctuations and is also observed in offshore environments [7]. Due to the time-varying nature of both wind magnitude and direction in turbulent conditions, UAVs may exhibit highly diverse and unpredictable landing trajectories.

Although most commercial UAVs report a wind resistance rating of up to 10 m/s [8], perfectly constant wind conditions are rarely observed in real-world environments [6]. Hence, most existing studies focus on reducing trajectory deviations under gust scenarios. Depending on the robustness of the controller and its compensation mechanisms, UAVs may recover their trajectories after such disturbances [9]. Most control approaches are based on Proportional-Integral-Derivative (PID) or Model Predictive Control (MPC) frameworks, enhanced with additional feedback, constraints, or compensation terms. These methods have been validated experimentally using high-power fans or through simulations with step-like gusts. More recently, reinforcement learning-based control strategies have also been explored and shown to be effective for mitigating gust-induced errors [10, 11].

However, simplified gust models with fixed direction and magnitude are insufficient to capture the complexity of the highly dynamic wind environment observed near offshore wind farms. For instance, the model in [11] introduces a linear ramp with Gaussian noise to simulate variability, but is limited to the horizontal plane and neglects vertical wind effects. In contrast, turbulent wind models incorporating time-varying fluctuations across three dimensions offer a more realistic representation of offshore wind environments.

Turbulent wind fields can be accurately simulated using computational fluid dynamics (CFD) [12], but the high computational cost makes CFD unsuitable for large-scale simulations required to assess the influence of descent speed and wind intensity on UAV landing performance.

To address this, many UAV studies adopt stochastic turbulence models based on power spectral density (PSD), such as the Dryden and von Kármán models [13, 14]. These models, grounded in stochastic theory and empirical data, provide a balance between accuracy and efficiency [6].

1.2 Summary of the Related Work

Section 1.1 reviews various wind field modelling approaches, as well as control and landing strategies to reduce landing errors. Table 1 summarises the key elements of the discussed UAV landing systems.

Most existing research on UAV landing strategies has concentrated on landing controllers for lightweight platforms ($\leq$2.5 kg) operating under unidirectional gust conditions, leaving three key gaps: (1) the influence of multidimensional variability in wind speed and direction on UAV landing accuracy has been largely overlooked; (2) the applicability of these strategies to high-payload UAVs remains uncertain; and (3) most importantly, except for the study by Olaz et al. [11], which specified a descent speed below 0.8 m/s, the role of descent speed in landing accuracy has been substantially underexplored, despite its direct impact on the UAV's exposure time to disturbances [5].

To address these gaps, this study develops integrated models of the UAV system and the three-dimensional turbulent wind field to provide a novel investigation into the effect of descent speed on the landing accuracy of high-payload UAVs under stochastic turbulent wind conditions.

2 DESIGN SPECIFICATIONS FOR UAV SAFE AND ACCURATE LANDING

Deploying IMR robots onto wind turbine blades using UAVs in turbulent environments requires the systematic quantification of key parameters related to the UAV platform, blade characteristics, environmental conditions, and the IMR robot. Currently, there is a lack of standardised design requirements for UAV landings on wind turbine blades under turbulent conditions. To ensure that the model aligns more closely with real-world offshore environments and application scenarios, this study proposes a set of design requirements for achieving safe and accurate UAV landings on wind turbine blades.

2.1 UAV platform and IMR robot specifications

A custom-built UAV platform named Goliath was developed in [3] for deploying a 4.5 kg IMR robot. Its capability to land on wind turbine blades was validated through field experiments under wind speeds of approximately 7.2 m/s and gusts reaching 9.2 m/s. The UAV was built upon a 3DXR-IND1000 octocopter frame with overall dimensions of 800 mm in width and depth and 500 mm in height. The UAV has an approximate mass of 14 kg. It was powered by eight X-U8II-KV85 motors equipped with MF2815 propellers, controlled via ALPHA 60A HV electronic speed controllers (ESCs), providing sufficient thrust to support a maximum take-off mass (MTOM) of approximately 30 kg.

2.2 Design requirements for Accurate and Safe Landing on Wind Turbine Blade Surface

In this study, wind turbine blades were designated as landing targets. Several design requirements were made based on a combination of existing literature, relevant regulations and standards, and field data collected from real-world offshore environments.

To ensure safe operation, the UAV must maintain a minimum stand-off distance of 5 m from the blade during inspection to prevent collision [19]. Therefore, the landing height range in this study was defined as a 5 m interval from the completion of the inspection to the landing on the blade surface. Furthermore, during the landing process, the UAV landing system should be capable of maintaining its attitude within 30 degrees even under variations in wind magnitude and direction [20].

A wind turbine blade can be divided into three sections: the root, the mid-section, and the tip [21]. While the root sec-

Table 1: Comparison of UAV landing systems in different wind conditions.

Study	Methodology	Wind type	Max. wind speed (m/s)	Landing error (mm)	System mass (kg)	Validation
Todeschini et al. [15]	MPC + hierarchical feedback controller	Constant wind (3D)	3.0	N/A	11.0	Simulation
Ghadiok et Al. [16]	Extensive filtering & altitude estimation	Gust (1D)	2.8	<500	1.4	Fan
Alexis et al. [14]	MPC + Piecewise Affine	Gust (3D)	4.3	N/A	2.5	Fan
Hentzen et al. [9]	MPC	Gust (1D)	12.0	<150.0	0.7	Fan
Mendez et al. [17]	Wind-preview-based MPC	Gust (1D)	10.0	<200.0	2.4	Simulation
Saj et al. [10]	RL	Gust (1D)	5.0	<50	1.4	Fan
Olaz et al [11]	RL	Gust (2D)	10.0	<500.0	N/A	Simulation
Sydney et al. [18]	Feedback linearisation controller	Turbulence (3D)	2.0	<400.0	N/A	Simulation

tion has the longest chord length, its high curvature makes it unsuitable for UAV landing due to the increased risk of flipping over. In contrast, the mid-section and tip have shorter chord lengths (approximately 2.7 m, based on the DTU 10-MW reference wind turbine [22]) but offer flatter surfaces.

To further enhance landing safety, operations near the blade edges should be avoided. A 0.2 m buffer zone was reserved on each side to reduce the risk of UAV fall-off, resulting in a defined landing zone width of 1.8 m, with 0.9 m on either side of the blade's central axis, as shown in Figure 2.

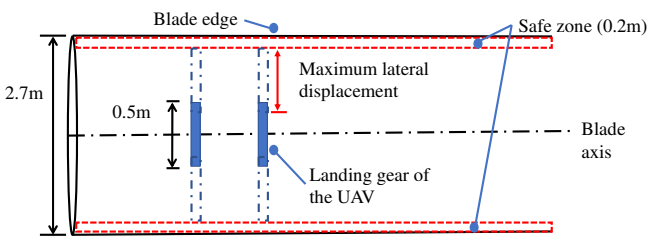

Figure 2: The illustration of the appropriate landing zone on the wind turbine blade surface and the maximum lateral displacement for the UAV to land accurately and safely on a wind turbine blade.

Offshore wind farms are subject to highly variable wind conditions, resulting in unpredictable wind speeds. To characterise typical conditions, a dataset of maximum wind speeds recorded from March to September 2013 at the Methil offshore wind farm, UK was analysed [3]. The results showed that wind speeds followed a normal distribution (7.82 ± 3.89 m/s). Wind speeds below 12 m/s account for 86.2% of all observations, supporting the selection of 12 m/s as the maximum threshold in this study.

3 UAV LANDING STRATEGY AND PLATFORM MODEL

3.1 *UAV Landing strategy*

Before modelling the UAV platform and the wind field, the UAV landing strategy must first be established. We assume that once the UAV carrying an IMR robot moves above the wind turbine blade, it has already identified a suitable landing spot during the scanning phase and hovers above it. After stabilising its attitude, the UAV accelerates from 0 m/s to the desired speed and then descends to the blade surface at this controlled speed through the wind field.

3.2 *UAV Platform Model*

The UAV platform model is based on the concepts presented in [20] and consists of four modules: kinematic, dynamic, control effectiveness, and propulsor models.

The UAV model is simplified as a six-degree-of-freedom (6-DOF) rigid body with four motors mounted in a cross configuration. Two right-handed coordinate frames of the Aircraft-Body Coordinate Frame (ABCF) and the Earth-Fixed Coordinate Frame (EFCF) are defined and denoted by the subscripts *b* and *e*.

3.2.1 UAV Kinematic Model

The position vector of the UAV's centre of mass (COM) is defined in the Earth-Fixed Coordinate Frame (EFCF) $\mathbf{p}_e = [x_e, y_e, z_e]^T \in \mathbb{R}^3$ with units of m, and its time derivative $\dot{\mathbf{p}}_e = \mathbf{v}_e$ represents the UAV's velocity in m/s.

The attitude of the UAV is represented using quaternions to avoid the singularity problem associated with Euler angle representations. The rotation from EFCF to ABCF is represented by $\mathbf{q}_e^b \triangleq [q_0\, q_1\, q_2\, q_3]^T \triangleq [q_0\, \mathbf{q}_V^T]^T$ (dimensionless, with $|\mathbf{q}_e^b| = 1$). The relationship between the quaternions and angular velocities of the UAV body can then be expressed as

$$\dot{\mathbf{q}}_e^b = \begin{bmatrix} \dot{q}_0 \\ \dot{\mathbf{q}}_V \end{bmatrix} = \frac{1}{2} \begin{bmatrix} -\mathbf{q}_V^T \\ q_0 \mathbf{I}_3 + [\mathbf{q}_V]_\times \end{bmatrix} \boldsymbol{\omega}_b, \tag{1}$$

where $\omega_b = [\omega_x\, \omega_y\, \omega_z]^T$ represents the angular velocity vector of the UAV body in rad/s, $\mathbf{I}_3$ is an identity matrix (dimensionless), and $[\mathbf{q}_V]_\times$ is the skew-symmetric form of $\mathbf{q}_V$ (dimensionless).

3.2.2 UAV Dynamic Model

The UAV dynamic model consists of translational and rotational representations, which are derived using the Newton-Euler equations [20]:

$$\dot{\mathbf{V}}_e = \begin{bmatrix} 0 \\ 0 \\ -g \end{bmatrix} + \frac{1}{m} R_b^e \begin{bmatrix} 0 \\ 0 \\ f_z \end{bmatrix} + \frac{1}{m} \begin{bmatrix} -k_x \dot{x}_e \\ -k_y \dot{y}_e \\ -k_z \dot{z}_e \end{bmatrix}, \tag{2}$$

http://www.imavs.org/

http://www.imavs.org/

$$J \cdot \dot{\omega}_b = -\omega_b \times (J \cdot \omega_b) + \boldsymbol{\tau}, \tag{3}$$

where g is the gravitational acceleration in m/s^2, m is the UAV mass in kg and f_z denotes the total thrust generated by the propellers in N. The coefficients k_x, k_y, k_z are dimensionless drag coefficients along the respective axes. $J = \mathrm{diag}(J_{xx}, J_{yy}, J_{zz}) \in \mathbb{R}^{3\times3}$ is the UAV's moment of inertia matrix with units of $kg \cdot m^2$, and the vector $\boldsymbol{\tau} \triangleq [\boldsymbol{\tau}_x\, \boldsymbol{\tau}_y\, \boldsymbol{\tau}_z] \in \mathbb{R}^3$ represents the body-frame torques generated by the propellers in $N \cdot m$.

The rotation matrix R_b^e from ABCF to EFCF was obtained from $\mathbf{q}_e^b$ using the standard conversion of quaternion to DCM (Direction Cosine Matrix). Both R_b^e and $\mathbf{q}_e^b$ are dimensionless. For simplicity, the gyroscopic torques generated by the spinning motors were neglected in this model.

3.2.3 Control effectiveness and propulsor model

The propeller thrust and dynamic reaction torque produced by each motor were modelled as:

$$T_i = C_T \varpi_i^2, \tag{4}$$

$$M_i = C_M \varpi_i^2 + J_{RP}\dot{\varpi}_i, \tag{5}$$

where C_T and C_M are the dimensionless coefficients of thrust and torque. The total thrust and torques of the UAV are then determined by the angular velocities of the propellers ϖ_i in rad/s:

$$\begin{bmatrix} f \\ \tau_x \\ \tau_y \\ \tau_z \end{bmatrix} = \begin{bmatrix} C_T & C_T & C_T & C_T \\ \frac{\sqrt{2}dC_T}{2} & \frac{-\sqrt{2}dC_T}{2} & \frac{-\sqrt{2}dC_T}{2} & \frac{\sqrt{2}dC_T}{2} \\ \frac{\sqrt{2}dC_T}{2} & \frac{\sqrt{2}dC_T}{2} & \frac{-\sqrt{2}dC_T}{2} & \frac{-\sqrt{2}dC_T}{2} \\ C_M & -C_M & C_M & -C_M \end{bmatrix} \begin{bmatrix} \varpi_1^2 \\ \varpi_2^2 \\ \varpi_3^2 \\ \varpi_4^2 \end{bmatrix}, \tag{6}$$

where d denotes the distance from each motor to the UAV's COM in m.

In turbulent environments, accurately modelling the motor's dynamic response is essential for capturing the UAV's real-time behaviour and landing performance. Therefore, this study incorporates both the motor and the ESC in the propulsor model. The ESC outputs a pulse width modulation (PWM) signal, which is converted to a dimensionless throttle command $\sigma \in [0, 1]$. At steady state, the motor speed ϖ_{ss} (in rad/s) is assumed to vary linearly with the throttle input:

$$\varpi_{ss}(\sigma) = C_R\sigma + \varpi_b,$$

where C_R and ϖ_b are the dimensionless gain and offset, respectively. To model the motor's response delay, a first-order dynamic response function with a time constant T_m is used, resulting in:

$$\varpi(s) = \frac{1}{T_m s + 1}(C_R\sigma + \varpi_b), \tag{7}$$

where T_m denotes the time required for the motor speed to reach 63.2% of its steady-state value (in s).

3.2.4 UAV control system

To evaluate the impact of descent velocity on UAV landing performance, a classic cascaded PID control system is adopted, commonly used in commercial UAVs [23]. The control system comprises four modules: position controller, attitude controller, motor controller, and the UAV platform model. The position controller includes vertical and horizontal sub-controllers.

The quadrotor UAV is an underactuated system with four control inputs—total thrust $f \in \mathbb{R}$ and body-axis torques $\boldsymbol{\tau} \in \mathbb{R}^3$—but six outputs: position $\mathbf{p} \in \mathbb{R}^3$ and attitude $\boldsymbol{\Theta} \in \mathbb{R}^3$. Consequently, only the desired position $\mathbf{p}_d$ and yaw angle Ψ_d are directly tracked, while the desired roll ϕ_d and pitch θ_d are computed from the horizontal position controller using the desired yaw angle and desired acceleration along the x and y axes.

Thrust and attitude commands are calculated by the PID controller and mapped to motor throttle inputs. To preserve attitude control margin, the thrust output was capped at 90% of the UAV's maximum capacity.

4 STOCHASTIC WIND TURBULENCE MODEL

As mentioned in Section 1.1, PSD-based methods are more suitable for simulating turbulent offshore environments for UAV landing scenarios. Compared to the Dryden model, the Von Kármán model shows better agreement with continuous turbulence measurements [24]. In this study, a stochastic wind turbulence model is constructed based on the Von Kármán model provided in the MATLAB/Simulink Aerospace Blockset (MIL-F-8785C).

4.1 Von Kármán Wind Turbulence Model

The von Kármán wind turbulence model generates time-varying wind velocities by applying frequency-domain turbulence filters to white noise inputs. These filters, defined as functions of the Laplace variable s, shape the spectral characteristics of wind disturbances in the longitudinal, lateral, and vertical directions. The corresponding transfer functions for each direction are given as follows:

$$\Phi_{V_{wind_u}}(s) = \frac{2\sigma_u^2 L_u}{\pi V} \cdot \frac{1}{\left[1 + \left(1.339\frac{L_u}{V}s\right)^2\right]^{5/6}} \tag{8}$$

$$\Phi_{V_{wind_v}}(s) = \frac{\sigma_v^2 L_v}{\pi V} \cdot \frac{1 + \frac{8}{3}\left(1.339\frac{L_v}{V}s\right)^2}{\left[1 + \left(1.339\frac{L_v}{V}s\right)^2\right]^{11/6}} \tag{9}$$

$$\Phi_{V_{wind_w}}(s) = \frac{\sigma_w^2 L_w}{\pi V} \cdot \frac{1 + \frac{8}{3}\left(1.339\frac{L_w}{V}s\right)^2}{\left[1 + \left(1.339\frac{L_w}{V}s\right)^2\right]^{11/6}}, \tag{10}$$

http://www.imavs.org/

where $\Phi_{V_{wind_u}}$, $\Phi_{V_{wind_v}}$, and $\Phi_{V_{wind_w}}$ are the power spectral densities of wind velocity in the x, y, and z directions, respectively. V represents the relative velocity between the UAV and the ambient wind. The parameters σ_u, σ_v, and σ_w indicate the turbulence intensities, while L_u, L_v, and L_w correspond to the turbulence scale lengths in each respective direction. These transfer functions are applied to white noise signals generated by a random source, producing fluctuations in external wind speed that characterise the temporal evolution of turbulence [25]. Different noise seeds yield distinct stochastic wind profiles.

According to the military specification MIL-F-8785C [26], the turbulence intensity σ and scale length L can be computed as functions of flight altitude h using the following:

$$\begin{aligned} L_w &= h, \\ L_u = L_v &= \frac{h}{(0.177 + 0.000823h)^{1.2}}, \end{aligned} \tag{11}$$

$$\begin{aligned} \sigma_w &= 0.1W_{20}, \\ \frac{\sigma_u}{\sigma_w} = \frac{\sigma_v}{\sigma_w} &= \frac{1}{(0.177 + 0.000823h)^{0.4}}, \end{aligned} \tag{12}$$

where h is the flight altitude of the UAV and W_{20} defines the average wind speed at 20 feet (6 m).

4.2 *Discrete Turbulent Wind Field Varying with Altitude*

In a classical von Kármán turbulence model, both mean wind speed and turbulence intensity are assumed constant. However, real wind farm environments exhibit vertical wind gradients, leading to varying wind speeds along the blade height, typically within 1 m/s per metre [27].

To capture this effect, the vertical space between the blade and the UAV is discretised into five uniform height intervals. Each interval is assigned a unique W_{20} to reflect local wind intensity. The wind speed at the mid-height is defined as V_{mid}, with random perturbations introduced via two sequences $\Theta_1 = [x_1, x_2, \ldots, x_{\frac{n}{2}}]$ and $\Theta_2 = [y_1, y_2, \ldots, y_{\frac{n}{2}}]$, where $0 < x_i < 1$ and $-1 < y_i < 0$. Wind speeds are increased above and decreased below the mid-level by sequentially adding these values, yielding a smoothly varying vertical wind profile, as illustrated in Figure 3.

5 SIMULATION SETUP AND METHODOLOGY SUMMARY

To evaluate whether higher descent speeds improve landing accuracy under turbulence, the UAV's descent velocity was varied from 0.5 m/s (a typical UAV landing speed [5]) to 3.0 m/s, the maximum descent speed limited by most commercial UAVs. Six discrete values: [0.5, 1.0, 1.5, 2.0, 2.5, 3.0] m/s were selected.

According to the design requirements in Section 2.2, the maximum wind speed is limited to 12 m/s. Since most UAVs

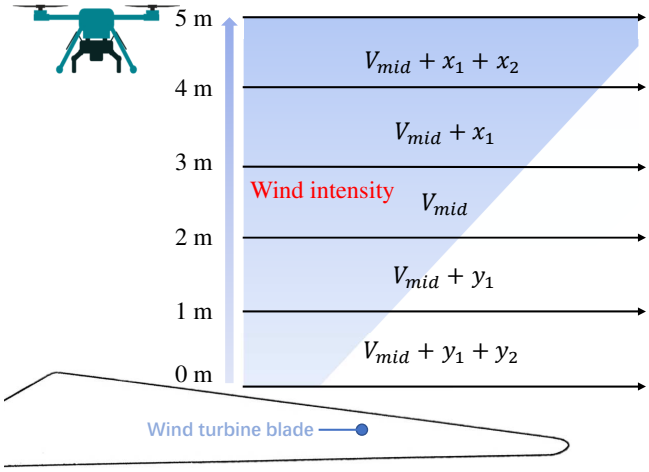

Figure 3: The illustration of the vertical wind gradients above the wind turbine blade.

can maintain landing accuracy under light breeze conditions (up to 3 m/s) [25], four representative values as [3.0, 6.0, 9.0, 12.0] m/s were selected for simulation.

Given the stochastic nature of the wind model, each simulation run generated a unique wind profile based on different random noise seeds. These seeds, along with the parameters Θ_1 and Θ_2, were recorded to ensure repeatability. For each wind speed setting, the same set of noise seeds was used across all descent speeds to enable a fair comparison.

Each combination of descent speed and wind speed was simulated 200 times, yielding a total of 4800 trials for statistical analysis. The choice of 200 trials per setting balances computational cost and statistical robustness, and is sufficient to capture the variability in landing outcomes caused by the stochastic wind conditions.

Simulations were conducted in MATLAB/Simulink using the ODE4 solver with a fixed time step of 0.001 s.

To provide a clearer overview of the simulation process, the integrated framework of the methodology is illustrated in Figure 4.

6 SIMULATION RESULTS AND DISCUSSION

In order to evaluate the UAV's landing accuracy and safety across varying wind speeds and descent velocities, this section considers the distribution of descent trajectories, the final touchdown locations, and the overall landing success rates under different scenarios.

6.1 *Landing trajectories*

In the process of UAV landing, maintaining a stable vertical descent trajectory is essential to avoid collisions with turbine structures. Figure 5 presents representative 3D landing trajectories for descent speeds of 0.5 m/s and 3.0 m/s under turbulent wind conditions with a maximum wind speed of 6 m/s.

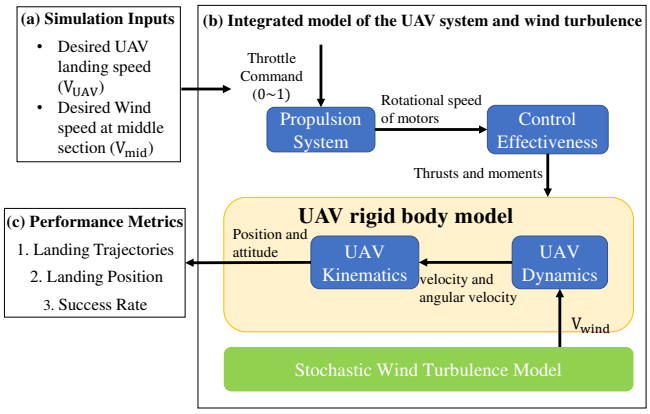

Figure 4: The summary diagram of the overall simulation flow, including (a) the simulation inputs; (b) the integrated model of the UAV system and the stochastic wind turbulence, where the wind model is embedded into the UAV dynamics; and (c) the performance metrics used to evaluate landing performance.

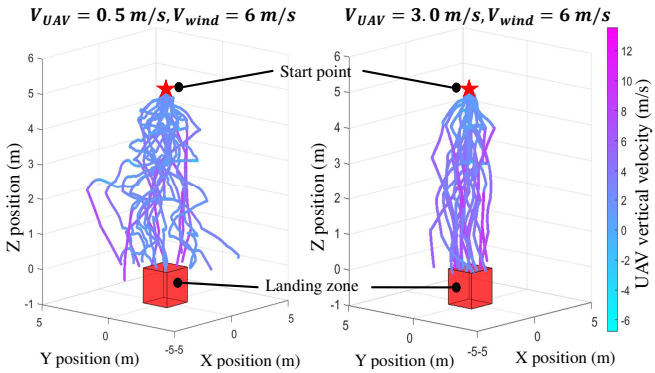

Figure 5: 20 samples of landing trajectories of UAV landing in 3D space when maximum wind speed is 6 m/s and a desired landing speed of 0.5 m/s and 3 m/s. The red box indicates the designated landing zone. The trajectories at 3.0 m/s are visibly more concentrated around the vertical descent path, while those at 0.5 m/s show greater lateral deviation. This suggests that descending at a higher speed in stochastic turbulent environments helps reduce the risk of collision with turbine structures.

The results show that despite the inherent randomness of the wind field, which could cause significant fluctuations in individual trajectories, a consistent overall descent pattern remained observable. A slower descent speed (0.5 m/s) leads to greater trajectory deviations, whereas a faster speed (3.0 m/s) results in trajectories more tightly concentrated around the vertical path. This also results in lower accuracy for the 0.5 m/s group, compared to the 3.0 m/s group, in terms of successfully reaching the designated landing zone.

The trajectories are colour-mapped according to the UAV's instantaneous descent speed, with visible colour fluctuations along some paths. These variations indicate disturbances in vertical motion caused by wind forces along the z-axis, which impair the UAV's ability to maintain its target descent speed.

6.2 *Landing position evaluation*

Figure 6 illustrates the landing positions of UAVs descending at speeds of 0.5 and 3.0 m/s under turbulent wind fields with maximum wind speeds of 3, 6, 9, and 12 m/s. Each marker represents the UAV's touchdown location on the turbine blade in a single simulation, while the red circle denotes the designated landing zone. The colour gradient of each point indicates its lateral displacement from the target, with lighter shades signifying a greater displacement.

All landing points exhibit a uniform radial distribution from the centre outward, suggesting the stochastic turbulent field affects the UAV symmetrically in all directions.

The results reveal that as wind speed increases, landing deviations become more pronounced, leading to more landings outside the designated target zone. However, across all wind conditions, UAVs descending at 0.5 m/s show a wider spread of landing positions and more outliers deviating from the central region. In contrast, at a descent speed of 3.0 m/s, the landing points are more concentrated near the centre. This improvement is particularly evident under wind speeds of 3.0 m/s and 6.0 m/s, with the most significant effect observed at 6.0 m/s, where the mean, median and standard deviations are reduced by 37.7%, 39.6% and 40.9%, respectively. However, under higher wind conditions (9.0 m/s and 12.0 m/s), the improvement diminishes, with the smallest gains observed at 12.0 m/s with reductions of 16.9%, 9.3% and 20.3%.

6.3 *Landing success rate*

Considering the safe landing zone defined in Section 2.2, Figure 6e presents a heat map illustrating the landing success rates across all tested scenarios. In every case, increasing the descent speed results in an improved success rate. Under relatively calm wind conditions with a maximum wind speed of 3 m/s, the UAV consistently maintained a success rate above 85%, reaching as high as 97.0% at a descent speed of 3.0 m/s—the highest success rate observed among all conditions. In contrast, within a 6 m/s wind field, the success rate only exceeded 50% when the descent speed was greater than 2.0 m/s; all other configurations failed to meet this threshold. However, the baseline success rate at 3 m/s wind speed was already high, resulting in relatively modest gains. Conversely, in the 6 m/s wind condition, the success rate improved significantly by approximately 30% as descent speed increased from 0.5 m/s to 3.0 m/s. This suggests that under moderately disturbed wind conditions, where UAV control is not completely compromised, increasing the descent speed can effectively enhance the probability of a successful and safe landing if the additional kinetic energy can be dissipated and

http://www.imavs.org/

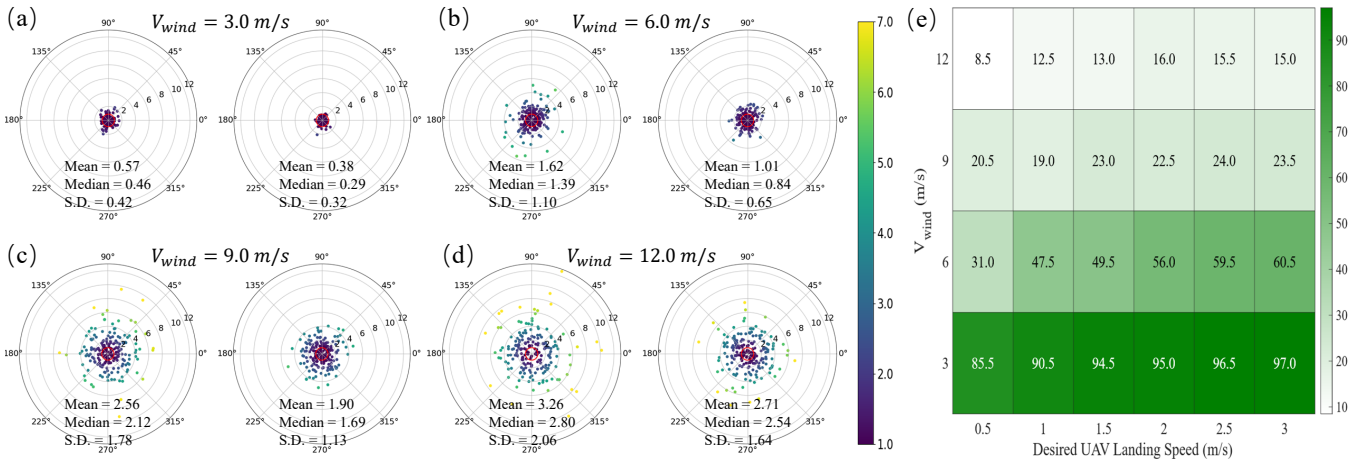

Figure 6: The bullseye graph displays the 200 samples of landing position of a UAV descending at 0.5 m/s and 3 m/s speeds in wind turbulence conditions of (a) 3 m/s, (b) 6 m/s, (c) 9 m/s, and (d) 12 m/s.

http://www.imavs.org/

not transferred to the wind turbine blades.

7 Conclusion and Future Work

In this study, we proposed a landing strategy that employs higher-than-typical UAV landing speeds to reduce landing errors in turbulent environments. The results have demonstrated that UAVs descending at higher speeds exhibit more stable and concentrated landing trajectories under identical maximum wind speed conditions, and can improve landing success rates by up to 30%. This offers a promising direction for enabling autonomous offshore wind turbine blade inspection, maintenance, and repair by multi-robot platforms.

Higher descent speeds cause a quadratic increase in kinetic energy. In this study, an 18.5 kg UAV descending at 0.5–3.0 m/s generates kinetic energy ranging from 2.3 J to 83.3 J, which may further increase under turbulence. If this energy exceeds the safe threshold for either the UAV or the wind turbine blade, structural damage may occur.

However, the structural interaction between UAVs and turbine blades was not comprehensively considered in this work, nor was the ground effect. Therefore, future investigations should incorporate detailed UAV–blade interaction models and aerodynamic effects near surfaces to define the safe threshold.

Building on this safe threshold, landing gear can be designed to dissipate excess energy, ensuring safer and more accurate landings. Current energy-absorbing systems for UAVs often introduce significant additional mass, which further elevates kinetic energy. As such, the development of lightweight landing gear with high energy absorption capacity presents a promising direction for future research.

Finally, this work was conducted solely in the simulation domain using MATLAB and SIMULINK toolboxes. Experimental validation under real-world field conditions is therefore necessary to confirm the applicability of the findings. Furthermore, the control analysis was limited to a classic PID controller, which constrains the scope of performance evaluation. Future work should explore more advanced controllers, such as Model Predictive Control (MPC), adaptive control, or learning-based approaches, both to rule out potential limitations of relying solely on a PID controller and to assess whether high-speed descent strategies can be extended to more severe turbulent environments.

References

[1] Ren21. *Renewables 2022 Global Status Report*. REN21 Secretariat, Paris, 2022.

[2] HF Zhou, HY Dou, LZ Qin, Y Chen, YQ Ni, and JM Ko. A review of full-scale structural testing of wind turbine blades. *Renewable and Sustainable Energy Reviews*, 33:177–187, 2014.

[3] Zhengyi Jiang, Ferdian Jovan, Peiman Moradi, Tom Richardson, Sara Bernardini, Simon Watson, Andrew Weightman, and Duncan Hine. A multirobot system for autonomous deployment and recovery of a blade crawler for operations and maintenance of offshore wind turbine blades. *Journal of Field Robotics*, 40(1):73–93, 2023.

[4] Yiming Liu, M Hajj, and Y Bao. Review of robot-based damage assessment for offshore wind turbines. *Renewable and Sustainable Energy Reviews*, 158:112187, 2022.

[5] John Bass, Isaac Tunney, and Alexis Lussier Desbiens. Adaptative friction shock absorbers and reverse thrust for fast multirotor landing on inclined surfaces. *IEEE Robotics and Automation Letters*, 7(3):6701–6708, 2022.

http://www.imavs.org/

[6] Bo Hang Wang, Dao Bo Wang, Zain Anwar Ali, Bai Ting Ting, and Hao Wang. An overview of various kinds of wind effects on unmanned aerial vehicle. *Measurement and Control*, 52(7-8):731–739, 2019.

[7] S Caires, J-J Schouten, L Lønseth, V Neshaug, I Pathirana, and O Storas. Uncertainties in offshore wind turbulence intensity. In *Journal of Physics: Conference Series*, volume 1356, page 012037. IOP Publishing, 2019.

[8] Mozhou Gao, Chris H Hugenholtz, Thomas A Fox, Maja Kucharczyk, Thomas E Barchyn, and Paul R Nesbit. Weather constraints on global drone flyability. *Scientific reports*, 11(1):12092, 2021.

[9] Daniel Hentzen, Thomas Stastny, Roland Siegwart, and Roland Brockers. Disturbance estimation and rejection for high-precision multirotor position control. In *2019 IEEE/RSJ International Conference on Intelligent Robots and Systems (IROS)*, pages 2797–2804. IEEE, 2019.

[10] Vishnu Saj, Bochan Lee, Dileep Kalathil, and Moble Benedict. Robust reinforcement learning algorithm for vision-based ship landing of uavs. *arXiv preprint arXiv:2209.08381*, 2022.

[11] Xabier Olaz, Daniel Alaez, Manuel Prieto, Jesús Villadangos, and José Javier Astrain. Quadcopter neural controller for take-off and landing in windy environments. *Expert Systems with Applications*, 225:120146, 2023.

[12] Craig WA Murray, Murray Ireland, and David Anderson. On the response of an autonomous quadrotor operating in a turbulent urban environment. In *AUVSI's unmanned systems conference*, 2014.

[13] Kenan Cole and Adam Wickenheiser. Spatio-temporal wind modeling for uav simulations. *arXiv preprint arXiv:1905.09954*, 2019.

[14] Kostas Alexis, George Nikolakopoulos, and Anthony Tzes. Constrained-control of a quadrotor helicopter for trajectory tracking under wind-gust disturbances. In *MELECON 2010-2010 15th IEEE Mediterranean Electrotechnical Conference*, pages 1411–1416. IEEE, 2010.

[15] Davide Todeschini, Lorenzo Fagiano, Claudio Micheli, and Aldo Cattano. Control of vertical take off, dynamic flight and landing of hybrid drones for airborne wind energy systems. In *2019 American control conference (ACC)*, pages 2177–2182. IEEE, 2019.

[16] Vaibhav Ghadiok, Jeremy Goldin, and Wei Ren. On the design and development of attitude stabilization, vision-based navigation, and aerial gripping for a low-cost quadrotor. *Autonomous Robots*, 33(1):41–68, 2012.

[17] Arthur P Mendez, James F Whidborne, and Lejun Chen. Wind preview-based model predictive control of multirotor uavs using lidar. *Sensors*, 23(7):3711, 2023.

[18] Nitin Sydney, Brendan Smyth, and Derek A Paley. Dynamic control of autonomous quadrotor flight in an estimated wind field. In *52nd IEEE Conference on Decision and Control*, pages 3609–3616. IEEE, 2013.

[19] C Galleguillos, A Zorrilla, Antonio Jimenez, L Diaz, ÁL Montiano, M Barroso, Antidio Viguria, and Fernando Lasagni. Thermographic non-destructive inspection of wind turbine blades using unmanned aerial systems. *Plastics, Rubber and Composites*, 44(3):98–103, 2015.

[20] Quan Quan. *Introduction to multicopter design and control*, volume 10. Springer, 2017.

[21] Amrit Shankar Verma, Jiquan Yan, Weifei Hu, Zhiyu Jiang, Wei Shi, and Julie JE Teuwen. A review of impact loads on composite wind turbine blades: Impact threats and classification. *Renewable and Sustainable Energy Reviews*, 178:113261, 2023.

[22] Christian Bak, Frederik Zahle, Robert Bitsche, Taeseong Kim, Anders Yde, Lars Christian Henriksen, Morten Hartvig Hansen, José Pedro Albergaria Amaral Blasques, Mac Gaunaa, and Anand Natarajan. The dtu 10-mw reference wind turbine, 2013. Danish Wind Power Research 2013 ; Conference date: 27-05-2013 Through 28-05-2013.

[23] Ivan Lopez-Sanchez and Javier Moreno-Valenzuela. Pid control of quadrotor uavs: A survey. *Annual Reviews in Control*, 56:100900, 2023.

[24] Frederic M Hoblit. Gust loads on aircraft: concepts and applications. 1988.

[25] Hyeongseok Kim, Daejin Lim, and Kwanjung Yee. Investigation of operable conditions and excess battery energy for quadrotors under wind turbulence. *Journal of Intelligent & Robotic Systems*, 104(3):52, 2022.

[26] US Military Specification: Flying Qualities of Piloted Airplanes. Technical Report MIL-F-8785C, Department of Defense, USA, November 1980. Military Standard.

[27] Siegfried Heier. *Grid integration of wind energy: onshore and offshore conversion systems*. John Wiley & Sons, 2014.